Inorganic Chemistry Research

Article

An Advanced Graphene Quantum Dot/NiFe-layered Double Hydroxide for Water Oxidation in a Neutral Solution

Leila Jafari Foruzin[a,*], Kamellia Nejati[b] and Zolfaghar Rezvani[a,*]

[a]*Department of Chemistry, Faculty of Basic Sciences, Azarbaijan Shahid Madani University, P.O. Box: 53714-161, Tabriz, Iran*

[b]*Department of Chemistry, Payame Noor University, P.O. Box: 19395-3697, Tehran, Iran*

Received: June 4, 2021; Accepted: August 3, 2021

Cite This: *Inorg. Chem. Res.* **2021,** *5*, 224-229. DOI: 10.22036/icr.2021.289233.1107

Abstract: Herein, it is reported that the nanocomposite of graphene quantum dot (GQD) and NiFe-layered double hydroxide (LDH) is a highly active and stable electrocatalyst for water oxidation. The GQD/NiFe-LDH composite was prepared using the hydrothermal method and investigated using X-ray diffraction (XRD) and Scanning electron microscopy (SEM). Based on the XRD and SEM results, the synthesis of GQD/NiFe-LDH was confirmed. Then, the GQD/NiFe-LDH composite was applied as an effective electrocatalyst for water oxidation. The obtained results from linear sweep voltammetry (LSV) curves show that GQD/NiFe-LDH improved water oxidation reaction with the overpotential of 323 mV in neutral media in comparison with pure NiFe-LDH, GQD, and RuO_2. The improved oxygen generation is due to the association of NiFe-LDH nano-plate with GQD. High activity of GQD/NiFe-LDH can be attributed to excellent electrical conductivity from GQD and high electrochemical activity due to the presence of NiFe-LDH. The stability of the electrocatalyst was investigated by water oxidation for 5.5 h.

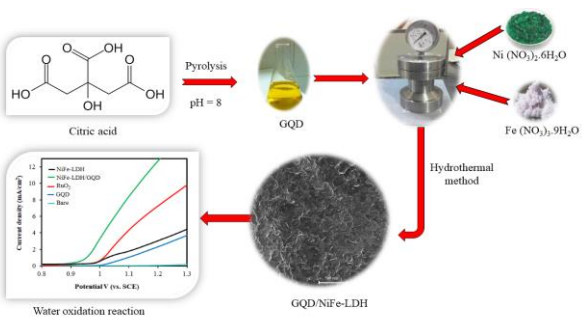

Keywords: Water oxidation, Graphene quantum dot, NiFe-layered double hydroxide, Nanocomposite

1. INTRODUCTION

Applying clean and renewable energy is considered as a way to decrease the use of fossil fuel. During recent years, an increase in alternative energy technology has improved in the area of water oxidation which acts as an energy transport.[1-3] O_2 generation is the technology of producing O_2 using electro-chemical water splitting and it contains storage energy and conversion energy.[4-5] Water oxidation needs a potential of about 1.23 V due to the slow kinetics of water oxidation.[6-7] An important challenge of O_2 generation is the use of efficient electrocatalysts which can decrease the time of reaction and reduce the energy used for water oxidation. The usual active electrocatalysts for water oxidation are iridium and ruthenium oxides but scarcity and high price of Ru and Ir make limited their use.[8-9] Many efforts have been made to use electrocatalysts based on first-row transition metal oxides and hydroxides.[10-12] Nevertheless, the water oxidation activity of these electrocatalysts is lower than that of IrO_2 and RuO_2. Therefore, applying cost-effective, stable, and highly active materials for water oxidation are still important factors. Many studies have been attracted a deal of notice to the graphene based materials such as graphene quantum dot (GQD) due to their high flexibility, electrical conductivity, and mechanical strength for several utilizations in the area of sensors, nanocomposite, nanoelectronics, and supercapacitors.[13-17] In general, a two-dimensional graphene for water oxidation with high efficiency has been studied. Nevertheless, the carbon atoms at graphene based materials caused lack of chemical reactivity. Hydrotalcite-like materials or layered double hydroxides (LDHs) have high chemical reactivity and are applied at several fields such as catalysts, photo-active, electrocatalyst, and anion exchangers.[18-22] Transition metals of LDHs caused improved water oxidation activity due to their good redox activity, low cost, and being eco-friendly.[23-24] So, synthesis of the GQD nanocomposite with LDH based materials will present an improved electrocatalyst with high electro-chemical activity in water oxidation. Also, the new composite has both complementary properties of graphene and LDHs. The LDHs will improve chemical activity while GQD can improve the electrical conductivity.[25-26] On the other hand, water oxidation in the alkali solution can destroy the system and device at a long period of time. So, water

oxidation at neutral or near neutral conditions was attractive in the most of studies during recent years.

Herein, we prepared GQD using pyrolysis of citric acid. Then, the GQD/NiFe-LDH nanocomposite was prepared using the hydrothermal method. After characterization of the prepared nanocomposite using scanning electron microscopy (SEM), X-ray diffraction (XRD), energy-dispersive X-ray (EDX) spectroscopy, and Fourier transform infrared spectroscopy (FT-IR), GQD/NiFe-LDH was applied as an excellent active electrocatalyst for water oxidation. It shows high water oxidation activity in neutral media with the small overpotential of 323 mV in neutral media (0.1 M phosphate sodium). Also, electrocatalytic activity of the GQD/NiFe-LDH composite is much better than that of RuO_2 electrocatalyst. The obtained nanocomposite possesses good electrocatalytic activity for water oxidation in neutral pH condition and provides low onset potential and stable operation for 5.5 h of water oxidation reaction.

2. EXPERIMENTAL

Synthesis of GQDs

The GQDs were obtained from pyrolysis of the citric acid (CA). GQD can be prepared by the following process. 5.3 g of CA was melted at a 50 mL beaker and the temperature was kept at 190 °C until the CA was converted into a yellow liquid at the carbonization process and carbon nanoparticles were produced after 30 min. Then the temperature was increased to 190 °C where the color of the liquid changed from yellow to orange, showing the complete formation of GQDs. Then, the pH of the obtained product was adjusted at 8 using NaOH solution (0.1 M). The obtained GQD was further purified by dialyzing it against water using a Spectra/Por dialysis membrane with molecular weight cut-off of 100 g mol^{-1} for 3 days. The obtained product was dried using the freeze dry method.

Synthesis of GQD/NiFe-LDH

The GQD/NiFe-LDH nanocomposite was synthesized by the hydrothermal method. In brief, 1.5 mg of GQD was dispersed in 20 mL of water and sonicated for 20 min. After that, 150 mL of 0.4 M $Ni(NO_3)_2.6H_2O$ and 0.1 M $Fe(NO_3)_3.9H_2O$ was added dropwise into a 20 mL GQD solution and the pH of the solution mixture was constant at 10.0 by using 1 M sodium hydroxide solution. The obtained product was transferred into the autoclave and kept at 60 °C for 24 h. The resulted product was centrifuged and then, washed with deionized water. The obtained chemical formula was GQD/Ni_4Fe-CO_3-LDH.

Synthesis of NiFe-LDH

NiFe-LDH was prepared by the hydrothermal method. NiFe-LDH was synthesized with 150 mL of 0.4 M $Ni(NO_3)_2.6H_2O$ and 150 mL of 0.1 M $Fe(NO_3)_3.9H_2O$ aqueous solution at pH = 10 using NaOH 1 M. Then the solution was kept at 60 °C for 24 h at the autoclave. The obtained NiFe-LDH was centrifuged and then, washed with deionized water.

Materials and characterization

Nickel nitrate ($Ni(NO_3)_2{\cdot}6H_2O$, 99.99%) and Iron nitrate ($Fe(NO_3)_3{\cdot}9H_2O$, 99.99%) were purchased from Sigma-Aldrich Chemical Company. RuO_2 was bought from Merck Company. All chemical materials were applied as purchased without purification.

The X-ray diffraction (XRD) patterns were recorded with a Bruker AXS model D8 Advance diffractometer using Cu-K_α radiation (λ = 1.542 Å) at 40 kV with the Bragg angle of 2-70°. The morphology of the prepared materials was investigated by scanning electron microscopy (SEM) (MIRA3 TESCAN scanning electron microscope) coupled with the energy-dispersive X-ray (EDX) Spectroscopy device. The UV–Vis absorption spectra were recorded using a T80 UV–Vis spectrophotometer model PG Instrument Ltd. Shimadzu FT-IR model Prestige 21 spectrometer was used to obtain the FT-IR spectra by the KBr method. The pH of solution was measured by a Hanna Instrument HI 2210 pH/C meter.

Electrochemical investigations were done using an AUTO LAB PGSTAT-100 potentiostat/galvanostat with a three electrode system. A glassy carbon electrode (GCE) (2 mm diameter), modified using the dropping method, was used as the working electrode. A Pt wire and a saturated calomel electrode (SCE) were used as the counter and reference electrodes, respectively. The surface of working electrode (GCE) was polished using a polishing paper and alumina paste to obtain a mirror-like surface. Then it was ultra-sonicated in a mixture of water and acetone solution with the volume ratio of 1:1. Then, 0.001 g of GQD/NiFe-LDH or RuO_2 and the mixture of 3 mL water were dispersed by the ultra-sonication method. Then, 5 µL of the prepared homogeneous solution was drop-casted onto GCE. The modified GCE was dried at room temperature.

3. RESULTS AND DISCUSSION

X-ray diffraction

The X-ray diffraction (XRD) patterns of GQD and the GQD/NiFe-LDH nano materials are presented in Figures 1(a) and (b). For the XRD pattern of GQD [see Figure 1(a)], the plane of graphene (002) as the broad peak is revealed at about 21.5° (d-space = 0.412 nm) which is due to their very small size. The obtained results show that d-space at GQD is smaller and higher than those of graphene oxide[27] and graphene, respectively, due to the presence of the functional groups at GQD.[28] As shown at Figure 1(b), the planes of (003), (006), (012), (015), and (110) are attributed to NiFe-LDH and no additional characteristic peaks appeared from the patterns, showing no impurities in NiFe-LDH.[29-30] The XRD patterns of the synthesized GQD/NiFe-LDH composite are in agreement with the standard cart of JCPDS 40-0215 with hexagonal lattice and R3m symmetry at NiFe-LDH and no characteristic peak of GQD is presented. Other studies also reported that at GQD, the diffraction peaks disappear or is weak if the exfoliation destroy the regular stacks of GQD.[31-32]

FT-IR spectra

Figure 2 shows the FT-IR spectra of NiFe-LDH, GQD, and GQD/NiFe-LDH. As shown in Figure 2(a), the broad band at 3400 cm^{-1} is related to the vibrations of the hydroxyl groups and intra-layer water molecules. The

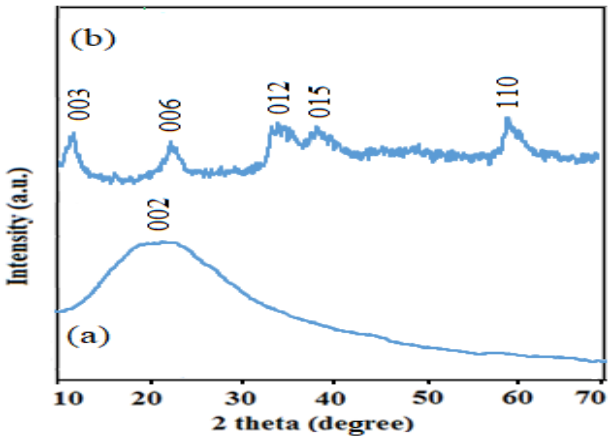

Figure 1. XRD patterns of (a) GQD and (b) GQD/NiFe-LDH.

band appearing in 1637 cm^{-1} corresponds to the vibrational model ν_1 of the interlayer water molecules. The peak in the region of 1384 cm^{-1} is related to the vibrations of the O–C–O group of the carbonate group and confirms the presence of carbonate ions between the LDH. The peaks appeared below 830 cm^{-1} are related to the metal-oxygen vibrations.[33] At Figure 2(b), the peak appearing in 3228 cm^{-1} is attributed to the O–H bond. The band appearing in 892 cm^{-1} is related to the C–H vibrations.[34] C=C vibrations appear in 1709 cm^{-1} and C–O–C bond vibrations appear in the wave number of about 1407 cm^{-1}.[35] Figure 2(c) shows the FT-IR spectrum of GQD/NiFe-LDH. In this figure, in addition to the NiFe-LDH peaks shown in Figure 2(b), the peak appearing in 2963 cm^{-1} is attributed to the C–H bond and the band appearing in 834 cm^{-1} is related to the C–H vibrations. The C–C vibrations appear in 1789 cm^{-1}. The C–O–C bond vibrations appear in 1098 and 1020 cm^{-1}.[36]

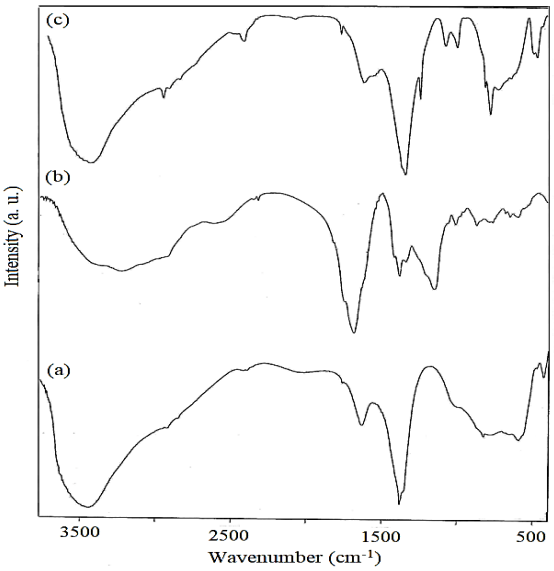

Figure 2. FT-IR spectra of (a) NiFe-LDH, (b) GQD, and (c) GQD/NiFe-LDH.

SEM image

The scanning electron microscopy (SEM) was used to study the morphology of the GQD/NiFe-LDH nanocomposite. The SEM image at Figure 3(a) shows that NiFe-LDH has plate-like morphology which is constructed via thin nano-plates with the thickness of about 20 nm. As shown in Figure 3(b), after synthesis of GQD/NiFe-LDH nanocomposit, the morphology is changed in compared with NiFe-LDH. It can be concluded that GQDs completely covers the surface of the plate like NiFe-LDH. The presence of Ni and Fe atoms in the prepared GQD/NiFe-LDH was confirmed by using the EDX analysis (Figure 4). As can be seen, the appeared characteristic atomic peaks associated with Fe and Ni demonstrate the preparation of NiFe-LDH; also, the present C atom confirms the synthesis of GQD.

.

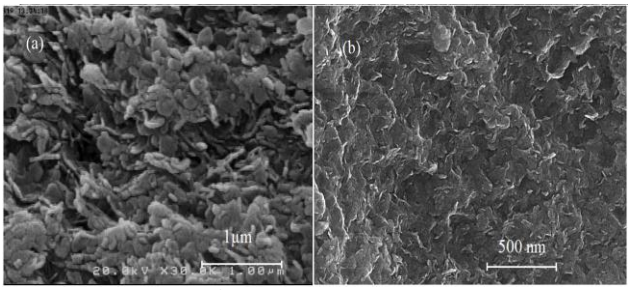

Figure 3. SEM images of (a) NiFe-LDH and (b) GQD/NiFe-LDH.

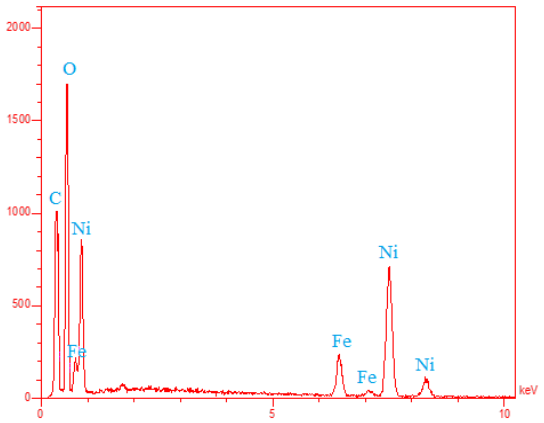

Figure 4. EDX analysis of GQD/NiFe-LDH.

UV-Vis spectra

The absorption (UV–Vis) spectrum of GQD is shown in Figure 5. According to the Figure, an absorbance peak was appeared at the wavelength of 240 nm which is attributed to the π–π* transitions of carbon= carbon. Also, a strong optical absorption was observed at UV-light (320 nm) which corresponded to the n–π* transition at the carbonyl group of GQD.[37] As shown in Figure 5, the absorbed intensity of GQD/NiFe-LDH, decreased due to quench effect of LDH. . Also, the d-d transitions of NiFe-LDH was occurred in the range of 370-700 nm.[38]

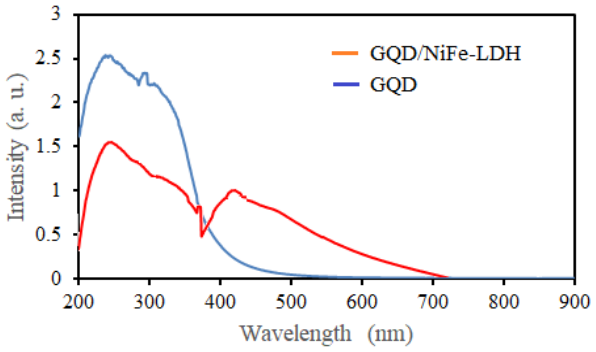

Figure 5. UV-Vis spectrum of GQD and GQD/NiFe-LDH.

Water oxidation

The electrocatalytic activity of the prepared materials was examined towards water oxidation in the neutral buffer media. The anodic currents of the NiFe-LDH, GQD, RuO_2, and GQD/NiFe-LDH electrocatalysts are presented in Figure 6. The LSV curve of the GQD/NiFe-LDH nanocomposite as the electrochemical catalyst was reported as the earliest onset potential at 0.9 V versus the reversible calomel electrode (SCE) in comparison with only NiFe-LDH, GQD, and RuO_2. Also, bare glassy carbon electrode has no water oxidation activity. So, this finding apparently reveals that the improved oxygen evaluation activity at the GQD/NiFe-LDH nanocomposite appeared from the strong dependence of GQD on NiFe-LDH, which further improved charge transport and increased catalytic activity. Furthermore, the applied overpotential for obtain the current density about 10 mA cm^{-2} presents the current density which was required for the convert of the solar energy into fuel with the efficiency of about 10% at the device.[39] So, it is an important factor at water oxidation. The current density of 10 mA cm^{-2} can be obtained at the overpotential of 550 mV for the GQD/NiFe-LDH catalyst. The overpotential for RuO_2 as the reference electrocatalyst was reported about 725 mV. Besides, the water oxidation activity of GQD/NiFe-LDH is much better than that of NiFe-LDH and GQD. Therefore, the result indicates that GQD/NiFe-LDH could efficiently improve the electrocatalytic activity of the water oxidation reaction.

In addition, the electrochemical impedance spectroscopy (EIS) was used for further corroboration of the obtained results and studying the charge transfer of GQD/NiFe-LDH. Figure 7 reports Nyquist plots of the GQD/NiFe-LDH and NiFe-LDH electrodes. In both samples, at the high frequency region, the plots contain a semicircle which is attributed to the charge-transfer resistance of the electrocatalyst.[40] According to Figure 7, the semicircle of NiFe-LDH is larger than that of GQD/NiFe-LDH. Based on these results, it is confirmed that GQD/NiFe-LDH has lower charge-transfer resistance. So, the charge transfer resistance at GQD/NiFe-LDH was smaller than that of NiFe-LDH. These results further indicate that the incorporation of GQD into NiFe-LDH caused improved conductivity and consequently, increased water oxidation activity at GQD/NiFe-LDH.

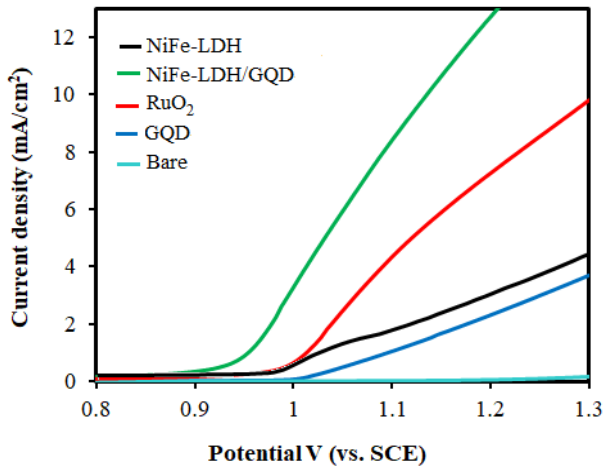

Figure 6. LSV curves of NiFe-LDH, GQD, GQD/NiFe-LDH, and RuO_2.

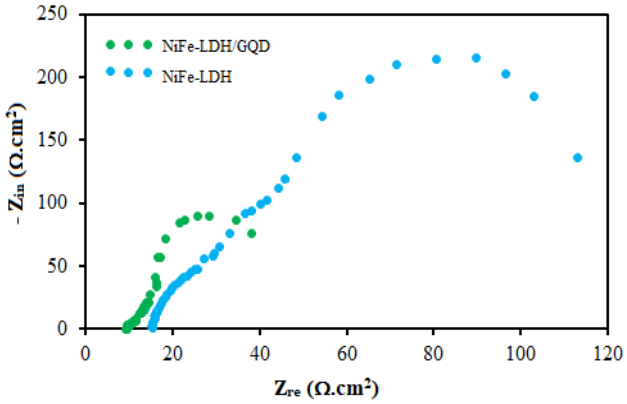

Figure 7. ESI curves of NiFe-LDH and GQD/NiFe-LDH.

In addition to the improved water oxidation activity, the GQD/NiFe-LDH catalyst also shows good durability for water oxidation. We investigated the stability of GQD/NiFe-LDH in a 0.1 M sodium phosphate buffer at the constant potential of 1.1 V versus SCE. Figure 8(I) shows that the GQD/NiFe-LDH composite had a current density of about 2.3 mA cm^{-2}. So, based on the chronoamperometry result, it can be confirmed that in addition to good water oxidation activity, the GQD/NiFe-LDH composite also shows suitable durability in neutral media. Furthermore, the XRD pattern (Figure 8(II)) and the corresponding EDX spectra after and before the OER test (Figures 8(III) and 8(IV), respevtively) show that initial crystallinity of the GQD/NiFe-LDH phase was stable and no changes were observed in GQD/NiFe-LDH after 5.5 h of water oxidation. To summarize the results, it can be concluded that an improved water oxidation

electrocatalyst with stable crystalline has been prepared. Also, all the data demonstrated that GQD/NiFe-LDH is an improved electrocatalyst with high stability in neutral media. The superb activity can be attributed to excellent electrical conductivity from GQD and high electrochemical reactivity due to the present NiFe-LDH. Table 1 summarizes the electrocatalytic activity of GQD/NiFe-LDH in comparison with the eelectrocatalyst reported in the literature.

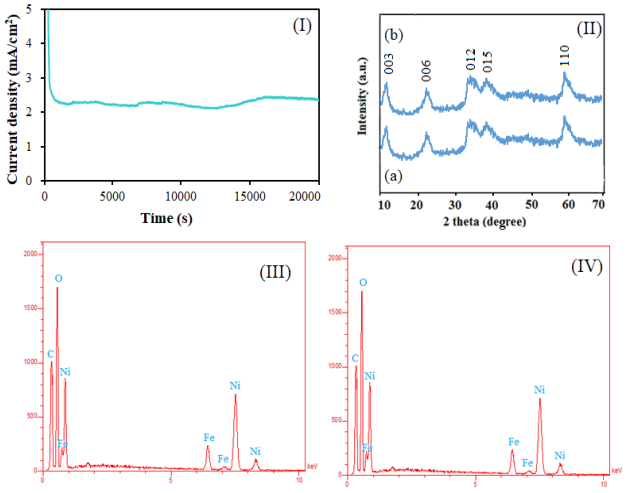

Figure 8. (I) Chronoamperogram curve of GQD/NiFe-LDH for water oxidation. (II) The XRD patterns of the GQD/NiFe-LDH through water oxidation [(a) Initial GQD/NiFe-LDH (b) after 5.5 h water oxidation]. (III) EDX analyzes of initial GQD/NiFe-LDH and (IV) after 5.5 h water oxidation.

Table 1. The electrocatalytic activity of GQD/NiFe-LDH in comparison with the electrocatalysts reported in the literature

Sample	pH	Overpotential (mV)	Ref.
Ni_2Fe-LDH-NO_3	7	420	41
Ni_3Fe-LDH-CO_3	7	425	42
CQD/NiFe-LDH	14	235	32
RGO/NiFe-LDH	13	250	43
NiFe-LDH	13	300	42
FeNi-GO LDH	14	210	44
GQD/NiFe-LDH	7	323	This study

4. CONCLUSIONS

The GQD nanoparticles were prepared through pyrolysis of CA as the precursors using a facile and rapid method at pH = 8. Then, GQD/NiFe-LDH as an active water oxidation electrocatalyst was synthesized by the hydrothermal method. The prepared material was characterized by the XRD, SEM, FT-IR, and EDX techniques. Based on the present study, inexpensive GQD/NiFe-LDH can improve water oxidation due to electron transport and it can increase conductivity with the onset potential of about 0.9 V vs. SCE and small overpotentials of 323 mV in the neutral solution (sodium phosphate 0.1 M), which is comparable or even better than that of the RuO_2 electrocatalysts. Furthermore, the chronopotentiometry tests with the GQD/NiFe-LDH composite catalyst revealed its good durability. This study proposes new insights into preparation of improved water oxidation electro-catalysts, which are strongly required for water oxidation reaction and energy conversion.

CONFLICTS OF INTEREST

The authors declare that they have no known competing financial interests or personal relationships that could have appeared to influence the work reported in this paper.

AUTHOR INFORMATION

Corresponding Author(s)

Leila Jafari Foruzin: Email: l.jafarie@gmail.com, ***ORCID***: 0000-0002-0211-9924

Zolfaghar Rezvani: Email: Z_rezvani@yahoo.com, ***ORCID***: 0000-0003-2157-7354

Author

Kamellia Nejati

ACKNOWLEDGEMENTS

The authors thank Azarbaijan Shahid Madani University and the Iran National Science Foundation (INSF) for financial supports.

REFERENCES

1. W. Zhang, W. Lai, R. Cao, *Chem. Rev.*, **2017**, *117*, 3717-3797.
2. Z. Zhang, T. Zheng, X. Li, J. Xu, H. Zeng, *Part. Part. Syst. Charact.*, **2016**, *33*,457-472.
3. S. Wan, J. Qi, W. Zhang, W. Wang, S. Zhang, K. Liu, H. Zheng, J. Sun, S. Wang, R. Cao, *Adv. Mater.*, **2017**, *29*, 1700286.
4. A. M. M. I. Qureshy, M. Ahmed, I. Dincer, *Int. J. Hydrogen Energy*, **2019**, *44*, 9237-9247.
5. S. Park, Y. Shao, J. Liu, Y. Wang, *Energy Environ. Sci.*, **2012**, *5*, 9331-9344.
6. H. Dau, C. Limberg, T. Reier, M. Risch, S. Roggan, P. Strasser, *Chem. Cat. Chem.*, **2010**, *2*, 724-761.
7. B. S. Yeo, A. T. Bell, *J. Phys. Chem. C*, **2012**, *116*, 8394-8400.
8. K. Liu, F. Wang, P. He, T. A. Shifa, Z. Wang, Z. Cheng, X. Zhan, J. He, *Adv. Energy Mater.*, **2018**, *8*, 1703290.
9. M. Liao, G. Zeng, T. Luo, Z. Jin, Y. Wang, X. Kou, D. Xiao, *Electrochim. Acta*, **2016**, *194*, 59-66.
10. M.S. Burke, L.J. Enman, A.S. Batchellor, S. Zou, S.W. Boettcher, Chem. Mater., **2015**, *27*, 7549-7558.
11. L. Zhang, Q. Fan, K. Li, S. Zhang, X. Ma, *Sustainable Energy Fuels*, **2020**, *4*, 5417-5432.
12. F. Lu, M. Zhou, Y. Zhou, X. Zeng, *Small*, **2017**, *13*, 1701931.

13. S. Sarabiyan Nejad, A. Babaie, M. Bagheri, M. Rezaei, F. Abbasi, A. Shomali, *Polym. Adv. Technol.*, **2020**, *31*, 2279-2289.
14. Y. R. Kumar, K. Deshmukh, K. K. Sadasivuni, S. K. K. Pasha, *RSC Adv.*, **2020**, *10*, 23861-23898.
15. F. Gao, C. -L. Yang, G. Jiang, *J. Photochem. Photobiol. A*, **2021**, *407*, 113080.
16. M. Wang, J. Fang, L. Hu, Y. Lai, Z. Liu, *Int. J. Hydrogen Energy*, **2017**, *42*, 21305-21310.
17. M. C. Daugherty, S. Gu, D. S. Aaron, R. E. Kelly, Y. Ashraf Gandomi, C. -T. Hsieh, *Nanoscale*, **2020**, *12*, 7834-7842.
18. N. Dewangan, W. M. Hui, S. Jayaprakash, A. -R. Bawah, A. J. Poerjoto, T. Jie, A. Jangam, K. Hidajat, S. Kawi, *Catal. Today*, **2020**, *356*, 490-513.
19. M. M. J. Li, C. Chen, T. Ayvalı, H. Suo, J. Zheng, I. F. Teixeira, L. Ye, H. Zou, D. O'Hare, S. C. E. Tsang, *ACS Catal.*, **2018**, *8*, 4390-4401.
20. J. J. Gil, O. Aguilar-Martínez, Y. Piña-Pérez, R. Pérez-Hernández, C. E. Santolalla-Vargas, R. Gómez, F. Tzompantzi, *Renewable Energy*, **2020**, *145*, 124-132.
21. H. S. Jadhav, A. Roy, B. Z. Desalegan, J. G. Seo, *Sustainable Energy Fuels*, **2020**, *4*, 312-323.
22. B. Ma, A. Fernandez-Martinez, S. Grangeon, C. Tournassat, N. Findling, S. Carrero, D. Tisserand, S. Bureau, E. Elkaïm, C. Marini, G. Aquilanti, A. Koishi, N. C. M. Marty, L. Charlet, *Environ. Sci. Technol.*, **2018**, *52*, 1624-1632.
23. S. Mallakpour, M. Hatami, *Polym.*, **2018**, *154*, 188-199.
24. H. Yuan, Y. Wang, C. Yang, Z. Liang, M. Chen, W. Zhang, H. Zheng, R. Cao, *Chem. Phys. Chem.*, **2019**, *20*, 2964-2967.
25. Y. -C. Chen, W. -H. Chiang, D. Kurniawan, P. -C. Yeh, K. -I. Otake, C. -W. Kung, *ACS Appl. Mater. Interfaces*, **2019**, *11*, 35319-35326.
26. A. Naddaf, S. Zeinali Heris, *Int. Commun. Heat Mass Transfer*, **2018**, *95*,116-122.
27. J. Peng, W. Gao, B. K. Gupta, Z. Liu, R. Romero-Aburto, L. Ge, L. Song, L. B. Alemany, X. Zhan, G. Gao, *Nano Lett.*, **2012**, *12*, 844-849.
28. C. Pang, S. Han, Y. Li, J. Zhang, *J. Chin. Chem. Soc.*, **2018**, *65*, 1504-1509.
29. Y. Gao, Z. Zhao, H. Jia, X. Yang, X. Lei, X. Kong, F. Zhang, *J. Mater. Sci.*, **2019**, *54*, 14515-14523.
30. S. Sanati, Z. Rezvani, *Ultrason. Sonochem.*, **2018**, *48*, 199-206.
31. C. Nethravathi, T. Nisha, N. Ravishankar, C. Shivakumara, M. Rajamathi, *Carbon*, **2009**, *47*, 2054-2059.
32. D. Tang, J. Liu, X. Wu, R. Liu, X. Han, Y. Han, H. Huang, Y. Liu, Z. Kang, *ACS Appl. Mater. Interfaces*, **2014**, *6*, 7918-7925.
33. D. Pan, S. Ge, J. Zhao, Q. Shao, L. Guo, X. Zhang, J. Lin, G. Xu, Z. Guo, *Dalton Trans.*, **2018**, *47*, 9765-9778.
34. S. Ramachandran, M. Sathishkumar, N. K. Kothurkar, R. Senthilkumar, *Mater. Sci. Eng.*, **2018**, *310*, 012139.
35. Z. -C. Yang, M. Wang, A. M. Yong, S. Y. Wong, X-H. Zhang, H. Tan, A. Y. Chang, X. Li, J. Wang, *Chem. Commun.*, **2011**, *47*, 11615-11617.
36. D. Arthisree, G. M. Joshi, *J. Mater. Sci.*, **2017**, *28*, 10516-10524.
37. J. P. Naik, P. Sutradhar, M. Saha, *J. Nanostruct. Chem.*, **2017**, *7*, 85-89.
38. S. Tonda, S. Kumar, M. Bhardwaj, P. Yadav, S. Ogale, *ACS Appl. Mater. Interfaces*, **2018**, *10*, 2667-2678.
39. L. -J. Zhou, X. Huang, H. Chen, P. Jin, G. -D. Li, X. Zou, *Dalton Trans.*, **2015**, *44*, 11592-11600.
40. J. Bao, Z. Wang, J. Xie, L. Xu, F. Lei, M. Guan, Y. Huang, Y. Zhao, J. Xia, H. Li, *Inorg. Chem. Front.*, **2018**, *5*, 2964-2970.
41. L. Jafari Foruzin, Z. Rezvani, B. Habibi, *Appl. Clay Sci.*, **2020**, *188*, 105511.
42. L. Jafari Foruzin, B. Habibi, Z. Rezvani, *New J. Chem.*, **2018**, *42*, 13963-13970.
43. D. -C. Xia, L. Zhou, S. Qiao, Y. Zhang, D. Tang, J. Liu, H. Huang, Y. Liu, Z. Kang, *Mater. Res. Bull.*, **2016**, *74*, 441-446.
44. X. Long, J. Li, S. Xiao, K. Yan, Z. Wang, H. Chen, S. Yang, *Angew. Chem.*, **2014**, *126*, 7714-7718.